Insertion of 3D DNA Origami Nanopores into Block Copolymer Vesicles

Saskia Groeer,[a, b, c] Martina Garni,[d] Avik Samanta,[f] and Andreas Walther*[e, f]

In memory of Prof. Wolfgang Meier

Block copolymer-based polymersomes are important building blocks for the bottom-up design of protocells and are considered advantageous over liposomes due to their higher mechanical stability and chemical versatility. Endowing both types of vesicles with capabilities for transmembrane transport is important for creating nanoreactor functionality and has been achieved by insertion of protein nanopores, even into comparably thick polymersome membranes. Still, the design space for protein nanopores is limited and higher flexibility might be accessible by de novo design of DNA nanopores, which have thus far been limited largely to liposome systems. Here, we introduce the successful insertion of two different 3D DNA origami nanopores into PMOXA-b-PDMS-b-PMOXA polymersomes, and confirm pore formation by dye influx studies and microscopy. This research thus opens the further design space of this versatile class of large DNA origami nanopores for polymersome-based functional protocells.

Introduction

Compartmentalization of intracellular machineries and metabolic processes is one of the central pillars of living systems and denotes a vital step in the emergence of extant life forms.[1] In order to obtain a fundamental understanding of biological systems and various life-defining processes, synthetic chemists

[a] Dr. S. Groeer
A³BMS Lab – Active, Adaptive and Autonomous Bioinspired Materials
Institute for Macromolecular Chemistry
University of Freiburg
Stefan-Meier-Straße 31, 79104 Freiburg (Germany)

[b] Dr. S. Groeer
Freiburg Materials Research Center (FMF)
University of Freiburg
Stefan-Meier-Str. 21, 79104 Freiburg (Germany)

[c] Dr. S. Groeer
Freiburg Center for Interactive Materials and
Bioinspired Technologies (FIT)
University of Freiburg
Georges-Köhler-Allee 105, 79110 Freiburg (Germany)

[d] Dr. M. Garni
Chemistry Department, University of Basel
BPR 1096, Postfach 3350, Mattenstrasse 24a,
4002 Basel (Switzerland)

[e] Prof. Dr. A. Walther
Cluster of Excellence livMatS @ FIT
79110 Freiburg (Germany)

[f] Dr. A. Samanta, Prof. Dr. A. Walther
A³BMS Lab – Active, Adaptive and Autonomous Bioinspired Materials
Department of Chemistry, University of Mainz
55128 Mainz (Germany)
E-mail: andreas.walther@uni-mainz.de
Homepage: https://www.walther-group.com

have been developing a wide range of protocellular confinements in bottom-up pathways using abiotic components with the ability to adapt and evolve.[2] In a proper protocellular model, it is crucial to engineering the semi-permeable membrane precisely since it serves in sequestration and protection of internal reactive components from the external environment as well as regulating the concentration gradients of the active materials or the flow of energy to perform work.[2a,3] Even though conventional lipid vesicles are commonly designated as one of the most credible predecessors of contemporary cells for their strong resemblance with the cellular membranes, in an application context, phospholipid membranes are however prone to chemical and mechanical membrane instability.[4] Additionally, transmembrane transportation of hydrophilic molecules (e.g., amino acids, phosphates, etc.) is in general restricted, even though this could be overcome in recent years by incorporating channel proteins[5] or entirely synthetic channels[6] in the membrane.

In contrast to liposomes, polymersomes consisting of amphiphilic block copolymers possess higher mechanical and chemical stability,[4a,7] and their higher membrane density and thickness retains even small molecules inside their cavity.[8] Additionally, the membrane properties are highly tunable by careful choice of the polymers used as well as the length of the hydrophilic and hydrophobic block. Membrane thicknesses can range from 5 nm to 50 nm.[9] Despite the thickness mismatch of protein nanopores and polymer membranes, there have been a few reports on the successful insertion of protein nanopores into polymersome membranes while keeping protein function intact.[10] Examples include in particular poly(dimethylsiloxane)-b-poly(2-methyl-2-oxazoline) (PDMS-b-PMOXA) polymers[10f,11] because the hydrophobic PDMS block is highly flexible with fluidity properties similar to phospholipid bilayers.[12] In this way, polymersomes can serve as versatile nanocontainers, nanoreactors, or for sensing applications.[9a] However, although protein nanopores can be genetically engineered to some

ChemSystemsChem

Research Article
doi.org/10.1002/syst.202200009

Chemistry Europe
European Chemical
Societies Publishing

degree, there is a limit to their possible modification in terms of chemistry and size.[5a,13] To expand functionalities of polymersomes, the *de novo* design of synthetic channels with predictable structures is highly desirable.[14]

Over the years, DNA has become one of the building blocks of choice for its predictability and programmability in designing hierarchical complex and intricate superstructures in bottom-up pathways. Recently, two approaches have been suggested to design artificial pores using DNA-based architectures:

(1) very small DNA nanobarrels assembled from a few individual strands and

(2) large DNA origami nanopores folded from a long DNA plasmid with the help of hundreds of staple strands.

The first strategy only requires a few DNA building blocks and may appear more straightforward; however, the second approach can generate significantly larger artificial pore constructs, which may be beneficial for bridging thicker membranes and building larger pores. Indeed, DNA origami nanopores with large diameters enable a broader range of molecules and even proteins to pass the membrane, allowing a broader range of analytes to be investigated or deliver more significant therapeutic agents. Recent research has presented a variety of DNA origami nanopores, including the first examples for signal-responsive pore formation.[15] The large body of work for both types of DNA nanopores has focused on implementing these nanopores into classical liposomes to achieve transmembrane transport[15b–d,16] or disrupt cellular function as antimicrobials.[17] In a recent report, DNA nanobarrels (strategy 1) were incorporated as transmembrane channels into the membrane of poly(2-(methacryloyloxy)ethyl phosphorylcholine))-*b*-poly((diisopropylamino) ethyl methacrylate) (PMPC-*b*-PDPA) polymersomes[14] in spite of the dimensional disparity between the pore length and membrane thickness. In contrast, the design principles for incorporating larger DNA origami nanopores (strategy 2) into block copolymer vesicle membranes remains elusive. Moreover, one has to appreciate that significantly different energetic situations may apply for inserting 3D origami channels into the membrane of polymersomes compared to liposomes because (i) brushy polymer layers provide additional entropic shielding, (ii) the hydrophobic membrane is significantly thicker, and (iii) the membranes have higher mechanical stability.[10b,18]

Herein, we set out to integrate large DNA origami constructs as nanopores into the membrane of polymersomes based on poly(2-methyl-2-oxazoline)-*b*-polydimethylsiloxane-*b*-poly(2-methyl-2-oxazoline) (=PMOXA-*b*-PDMS-*b*-PMOXA) – a widely used block copolymer for the design of synthetic organelles.[11c,19] Two cholesterol-modified DNA origami with different pore sizes and stem lengths are designed for insertion into the block copolymer membranes, and their integration with the polymersome membrane is investigated. TEM and CLSM demonstrate integration into the block copolymer membrane, and the functionality of the assembled protocells regarding the operation of the pore is demonstrated by the use of dye influx upon pore formation. This all-synthetic approach lays essential groundwork for mechanically stable, functional protocell models, using straightforward assembly principles and robust building blocks.

Results and Discussion

In order to engineer a DNA origami capable of forming channels through a polymer membrane, we devised an origami structure consisting of a thin protruding stem part constituting the actual pore size and a larger barrel-shaped top part, resembling the protein nanopore composed of α-hemolysin.[20] Two different origami structures are synthesized: (1) A larger and more rigid nanopore (NP$_{large}$, Figure 1a) and (2) a more slender, long, and flexible nanopore with a smaller pore diameter (NP$_{small}$, Figure 1b). The stem is designed to orient and stabilize inside the membrane by hydrophobic cholesterol anchors at the bottom end of the barrel-shaped top part. The amount of cholesterol sufficient for energetic compensation during pore formation was estimated based on DNA origami insertion data into liposomes,[15c] which is only an approximation for polymer membranes. The large top cavity of the nanopore has the advantage of enabling the anchorage of enzymes or other catalysts for use as nanoreactors in future research. Both DNA origami nanopores were folded using an annealing ramp with the respective scaffold and staple strands at 22 mM MgCl$_2$ and 5 mM NaCl.

In more detail, NP$_{large}$ in Figure 1a uses an 8064 nb scaffold strand and has six ssDNA overhangs at the top for modification with ATTO 488 dye. At the bottom of the cavity around the protruding stem, there are 66 ssDNA overhangs for modification with complementary cholesterol-ssDNA (added after folding at 30°C). Figure 1a summarizes the expected dimensions. Transmission electron microscopy (TEM) allows verification of the nanopore's dimensions (Figure 1d). The stem length is slightly shorter in TEM (10 nm) due to drying artifacts with the barrel obstructing stem parts. Note that the stem length is designed to avoid size mismatches with the polymer membrane (see below).[12a] The double-walled design of the stem grants additional rigidity. NP$_{small}$ uses a 7249 nb scaffold and is similarly equipped with six ssDNA overhangs for dye modification and 33 ssDNA overhangs for cholesterol modification (Figure 1b). Its stem is thinner with an outer diameter of 6 nm due to a single-walled design and longer (26 nm) to be more flexible and allow full membrane piercing. TEM visualizes a stem length of ca. 21 nm (Figure 1e).

Further TEM characterization confirms a correct and homogenous folding of both nanopores; however, the visualization of the thin stem of the NP$_{small}$ is challenging due to some lack of contrast in the micrographs. The origami folding map and all sequences used are shown in Figure S1 to Figure S3 and Table S1 to S9 in the Supporting Information.

All polymersomes used in this study are based on PMOXA$_6$-*b*-PDMS$_{65}$-*b*-PMOXA$_6$, a commercially available block copolymer interesting due to its high membrane fluidity (glass transition temperature of PDMS = −123 °C),[21] which is theorized to facilitate pore insertion.[12a] This polymer is known to form polymersomes with a membrane thickness of ca. 14 nm.[12a] Two
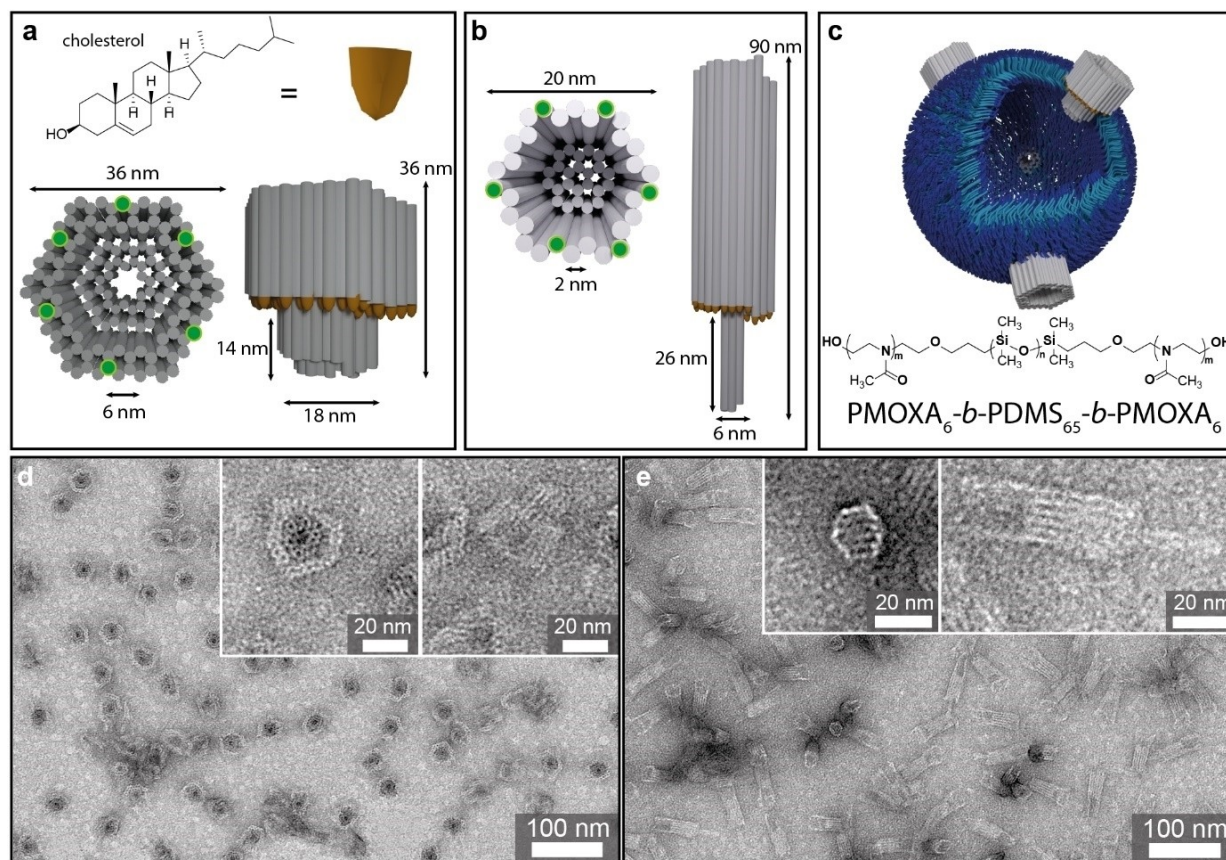
Figure 1. DNA origami nanopores for insertion into polymersomes. (a) Schematic view of NP_{large} with 66 cholesterol anchors (orange) and six ATTO 488 (green), 6 nm pore diameter. (b) Schematic view of NP_{small} with 33 cholesterol anchors (orange) and six ATTO 488 (green), 2 nm diameter. (c) Scheme of a $PMOXA_6$-b-$PDMS_{65}$-b-$PMOXA_6$ triblock-copolymer-based polymersome with large origami nanopores inserted. (d) TEM image of NP_{large}. (e) TEM image of NP_{small}.

different populations of polymersomes can be formed: (1) small nanoscale polymersomes, termed small unilamellar vesicles (SUVs), form under stirring in a sucrose solution and subsequent extrusion (Figure 2a) with z-average diameters, d, of 150 nm (dispersity, $D = 1.2$) as measured using dynamic light scattering (DLS), and (2) large micrometer-sized polymersomes, termed giant unilamellar vesicles (GUVs), are accessible by thin-film rehydration with a sucrose solution in the absence of stirring (Figure 2b). Sucrose supports vesicle growth and allows vesicles to sink to the bottom if diluted in imaging buffer, facilitating
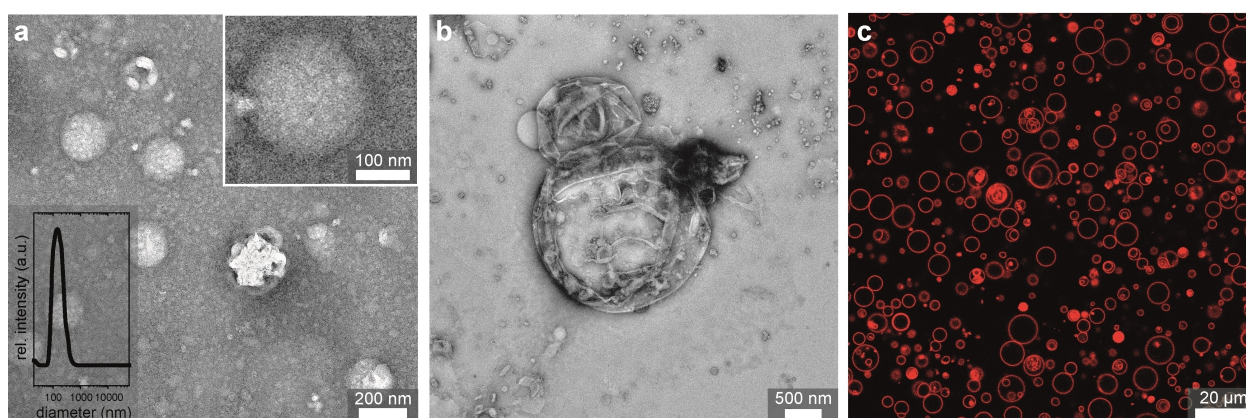

Figure 2. Characterization of polymersomes. (a) TEM image of $PMOXA_6$-b-$PDMS_{65}$-b-$PMOXA_6$ SUVs. Inset: DLS CONTIN distribution of the SUV diameter. (b) TEM image of $PMOXA_6$-b-$PDMS_{65}$-b-$PMOXA_6$ GUVs. (c) CLSM image of $PMOXA_6$-b-$PDMS_{65}$-b-$PMOXA_6$ GUVs stained with Bodipy dye.

later confocal laser scanning microscopy (CLSM) studies.[22] The TEM characterization shows collapsed vesicles with a relatively broad size distribution. Both multilamellar and multi-vesicular vesicles can be identified as well, as further confirmed by CLSM imaging by staining the membrane with Bodipy dye (Figure 2c). The diameters range between 1–20 μm.

To enable the insertion of the DNA origami nanopores into the polymersomes, they are decorated with cholesterol by which they are supposed to adhere and insert into the polymersome membrane. Reorientation of the nanopore then causes their stems to penetrate the membrane allowing molecular transport across the membrane boundaries. We verified each of these steps by thorough investigations using agarose gel electrophoresis (AGE), TEM, and CLSM, including dye influx studies.

Attachment of the cholesterol-ssDNA strands to the nanopores and subsequent interaction of the modified nanopores to the polymersomes was first investigated with the SUVs using AGE and TEM (Figure 3). The unmodified DNA origami displays sharp bands in AGE (lanes 1–2), proving the successful folding of the structures (Figure 3a). Strong smearing of the nanopore bands occurs after cholesterol modification (lane 3–4) and is caused by the hydrophobic anchors slowing down the electrophoretic mobility. This confirms the attachment of the cholesterol to the origami. Once the nanopores are mixed with SUVs, any migration of the DNA origami nanopores into the gel is stopped entirely, and the origami-functionalized polymersomes remain in the pockets of the gel (lane 5–6). Gratifyingly, TEM analysis in Figure 3b shows a polymersome with a membrane fully covered by NP$_{large}$, although their orientation cannot be fully identified. Moreover, further insight is gained by a closer inspection of the pore orientation of NP$_{small}$ (Figure 3c) from a higher magnified TEM micrograph. The orientation of the barrel-shaped top part facing away from the polymersome membrane suggests that the stem part of the origami faces the membrane (inset), thereby indicating successful channel formation onto the polymersome membrane.

Finally, to confirm that the cholesterol anchor-driven membrane adhesion leads indeed to transmembrane channel formation, we studied real-time CLSM monitoring of sulforhodamine B (SRB, laser excitation = 522 nm; red channel) influx into the GUVs decorated with ATTO 488-labeled origami nanopores (laser excitation = 488 nm; green channel) as a proof-of-concept set up. Notably, the osmolarity of the solution is kept constant to prevent osmotic shock and GUV breakdown. As a control experiment, we mixed nanopores without cholesterol modification with the GUVs. In a series of control experiments, we observed that DNA origami nanopores without cholesterol tags do not interact with the polymersome membrane, and the nanopores are evenly distributed in the solution (Figure 4a,c). No accumulation of a green signal at the polymersome membrane is observed. In stark contrast, NP$_{large}$ modified with cholesterol adheres to the polymersome membrane within one minute (Figure 4b), leading to an increased ATTO 488 fluorescence and a corresponding maximum in the greyscale values at the vesicle membrane. Similar results are found for NP$_{small}$, which, when decorated with cholesterol, also assembles to the polymersome membrane within one minute (Figure 4d).

The influx of SRB into GUVs is monitored over time to confirm pore formation. First, the SBR is added to a polymersome solution, and then the DNA origami nanopores are added. Figure 4e shows a successful influx of SRB after ca. 70 min for NP$_{large}$. This confirms that DNA origami channels assist the transmembrane transportation of the hydrophilic dye molecules. The time difference between rapid adsorption at the membrane and delayed functional pore built-up is on par with the liposome studies where a two-stage mechanism has been discussed: first, the nanopore attaches to the bilayer membrane *via* the cholesterol anchors, after which reorientation to form pores occurs in a delayed, yet sudden fashion.[15c] The selected image series also depicts a vesicle that turns out to be a multi-vesicular structure, in which the parent GUV hosts three small GUVs inside its core. This example confirms that indeed the DNA origami nanopores are responsible for dye influx, because it
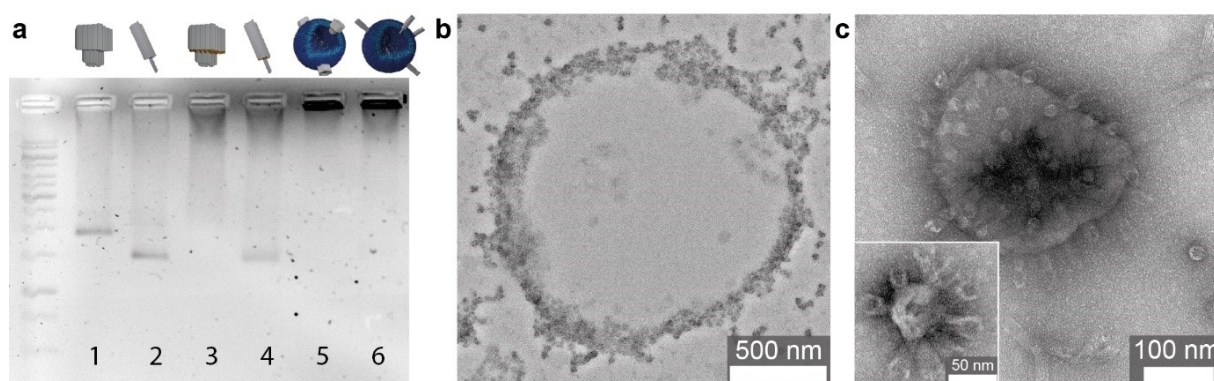

Figure 3. Characterization of DNA origami nanopores and insertion into polymersomes. (a) AGE of DNA origami nanopores (1.5 wt% agarose in TBE buffer, stained with ROTIGelStain, 1 kbp DNA ladder). 1: NP$_{large}$ without cholesterol anchors. 2: NP$_{small}$ without cholesterol anchors. 3: NP$_{large}$ with 66 cholesterol anchors. 4: NP$_{small}$ with 33 cholesterol anchors. 5: NP$_{large}$ with cholesterol anchors mixed with SUVs. 6: NP$_{small}$ with cholesterol anchors mixed with SUVs. (b) TEM image of a polymersome with NP$_{large}$. (c) TEM images of polymersomes with NP$_{small}$.
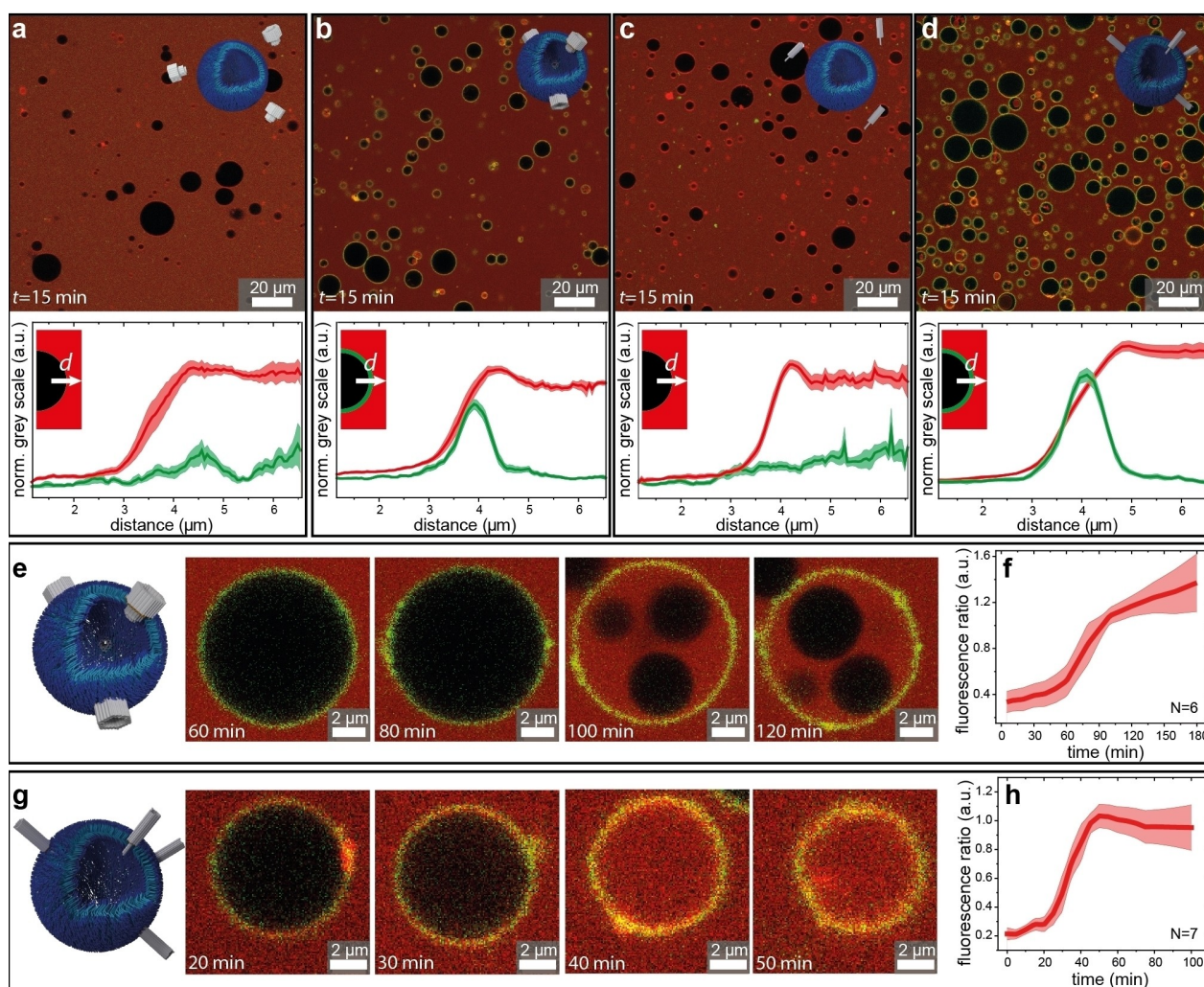
ChemSystemsChem

Research Article
doi.org/10.1002/syst.202200009

Chemistry Europe
European Chemical
Societies Publishing

Figure 4. CLSM characterization of SRB dye influx (red channel) into $PMOXA_6$-b-$PDMS_{65}$-b-$PMOXA_6$ GUVs after pore formation of origami nanopores (green channel). (a-b) CLSM of GUVs mixed with NP_{large} (a) without and (b) with cholesterol anchors after 15 min. (c-d) CLSM of GUVs mixed with NP_{small} (c) without and (d) with cholesterol anchors after 15 min. (a-d) Bottom: Normalized greyscale values across the vesicle membrane along the distance d averaged over 10 vesicles for the red channel (red line) and the green channel (green line). (e,g) CLSM images of SRB influx into a GUV after pore formation of (e) NP_{large} and (g) NP_{small}. (f,h) Fluorescence ratio of fluorescence inside and outside GUVs over time as measured with CLSM for (f) NP_{large} and (h) NP_{small}. Shaded areas depict standard errors of the curves averaged over (a-d) 10 vesicles or (f-h) N influx events.

can only take place through the outer vesicular membrane, as the origami nanopores can only access the outer membrane. Such multi-vesicular structures also explain the increase of the fluorescence ratio above 1 in Figure 4f, as the scattering of especially multi-vesicular structures can lead to an increased fluorescence signal.

Similarly, Figure 4g confirms dye influx into GUVs mixed with NP_{small} as well. Pore formation sets in faster with dye influx taking place after ca. 30 min (Figure 4h, Movie S1). This shows how either stem size or hydrophobic tag density influence the kinetics of pore formation. While both pores show very fast adhesion to the GUV membrane, reorientation of the origami to form a pore happens slowly, and it is size-dependent, with thinner stems favoring faster reorientation. The fact that adsorption happens fast, whereas dye leakage is a delayed process also confirms that adsorption

alone does not disrupt the membrane. In summary, both systems provide compelling evidence for the successful pore formation in thick block copolymer membranes, resulting in a functional synthetic protocell that enables dye flux across the polymersome membrane and thus mimics protein nanopore functions in a biological cell.

Conclusion

In summary, we introduced the concept of integrating 3D DNA origami nanopores with tunable structure into mechanically robust triblock copolymer polymersomes with comparably thick membrane walls. Two sets of origami nanopores with varying stem diameters were designed, annealed, and equipped with fluorophores for CLSM visual-

ChemSystemsChem

Research Article
doi.org/10.1002/syst.202200009

Chemistry Europe
European Chemical
Societies Publishing

ization. Successful immobilization and pore formation could be shown after a dense functionalization via cholesterol tags to compensate for the energy during pore formation and to anchor the origami inside the polymer membrane by hydrophobic interactions. According to the dye influx and CLSM imaging data, pore formation is a two-step mechanism with quick adhesion and subsequent reorientation and pore formation. This process depends on the size of the nanopore but has proven to be sufficiently robust, as it is shown for two different nanopore constructs. A thin stem, albeit a lower density of cholesterol anchors, facilitates a quicker reorientation inside the membrane.

The study established the basic principles to introduce DNA origami nanopores to the field of block copolymer vesicles, their nanoreactors, or protocellular entities. The hybrid structures presented in this study can be further expanded by modifying the nanopores with a trigger-responsive cap for controlled release using DNA keys,[15c,16a] temperature[16b] or pH (e.g. using triplex structures) as a trigger, thus endowing polymersome-based structures with new functionalities often not accessible using classical functionalization principles. Looking out to the future, it will be relevant to study the robustness of pore formation targeting polymersomes of completely different chemistry (e.g., higher glass transition temperature, charge soluble blocks), and to understand how membrane thickness scales with the propensity with pore formation.

Acknowledgments

Conflict of Interest

The authors declare no conflict of interest.

Data Availability Statement

The data that support the findings of this study are available from the corresponding author upon reasonable request.

Keywords: Artificial cells · DNA origami · nanopores · vesicles · polymersomes

[1] a) D. E. Koshland, *Science* **2002**, *295*, 2215–2216; b) S. Mann, *Acc. Chem. Res.* **2012**, *45*, 2131–2141.

[2] a) J. W. Szostak, D. P. Bartel, P. L. Luisi, *Nature* **2001**, *409*, 387–390; b) Y.-C. Lai, I. A. Chen, *Curr. Biol.* **2020**, *30*, R482-R485; c) A. J. Dzieciol, S. Mann, *Chem. Soc. Rev.* **2012**, *41*, 79–85; d) A. Samanta, V. Sabatino, T. R. Ward, A. Walther, *Nat. Nanotechnol.* **2020**, *15*, 914–921; e) S. Ludwanowski, A. Samanta, S. Loescher, C. Barner-Kowollik, A. Walther, *Adv. Sci.* **2021**, *8*, 2003740.

[3] R. J. Peters, M. Marguet, S. Marais, M. W. Fraaije, J. C. van Hest, S. Lecommandoux, *Angew. Chem. Int. Ed.* **2014**, *53*, 146–150; *Angew. Chem.* **2014**, *126*, 150–154.

[4] a) L. Messager, J. Gaitzsch, L. Chierico, G. Battaglia, *Curr. Opin. Pharmacol.* **2014**, *18*, 104–111; b) D. D. Lasic, D. Papahadjopoulos in *Medical Applications of Liposomes*, 1st ed. Elsevier, Amsterdam, **1998**, p. 779.

[5] a) M. Mayer, J. Yang, *Acc. Chem. Res.* **2013**, *46*, 2998–3008; b) Z. Zhang, X. Huang, Y. Qian, W. Chen, L. Wen, L. Jiang, *Adv. Mater.* **2019**, e1904351.

[6] a) U. Kauscher, A. Samanta, B. J. Ravoo, *Org. Biomol. Chem.* **2014**, *12*, 600–606; b) M. Yano, C. C. Tong, M. E. Light, F. P. Schmidtchen, P. A. Gale, *Org. Biomol. Chem.* **2010**, *8*, 4356–4363; c) A. Roy, J. Shen, H. Joshi, W. Song, Y.-M. Tu, R. Chowdhury, R. Ye, N. Li, C. Ren, M. Kumar, A. Aksimentiev, H. Zeng, *Nat. Nanotechnol.* **2021**, *16*, 911–917.

[7] a) J. C. Lee, H. Bermudez, B. M. Discher, M. A. Sheehan, Y. Y. Won, F. S. Bates, D. E. Discher, *Biotechnol. Bioeng.* **2001**, *73*, 135–145; b) H. Bermudez, A. K. Brannan, D. A. Hammer, F. S. Bates, D. E. Discher, *Macromolecules* **2002**, *35*, 8203–8208.

[8] C. LoPresti, H. Lomas, M. Massignani, T. Smart, G. Battaglia, *J. Mater. Chem.* **2009**, *19*.

[9] a) C. G. Palivan, R. Goers, A. Najer, X. Zhang, A. Car, W. Meier, *Chem. Soc. Rev.* **2016**, *45*, 377–411; b) F. Li, S. Prévost, R. Schweins, A. T. M. Marcelis, F. A. M. Leermakers, M. A. Cohen Stuart, E. J. R. Sudhölter, *Soft Matter* **2009**, *5*, 4169–4172; c) Q. Chen, H. Schönherr, G. J. Vancso, *Soft Matter* **2009**, *5*, 4944–4950.

[10] a) M. Lomora, M. Garni, F. Itel, P. Tanner, M. Spulber, C. G. Palivan, *Biomaterials* **2015**, *53*, 406–414; b) A. Belluati, V. Mikhalevich, S. Yorulmaz Avsar, D. Daubian, I. Craciun, M. Chami, W. P. Meier, C. G. Palivan, *Biomacromolecules* **2020**, *21*, 701–715; c) H. J. Choi, C. D. Montemagno, *Nano Lett.* **2005**, *5*, 2538–2542; d) A. Picker, H. Nuss, P. Guenoun, C. Chevallard, *Langmuir* **2011**, *27*, 3213–3218; e) M. Kumar, M. Grzelakowski, J. Zilles, M. Clark, W. Meier, *Proc. Nat. Acad. Sci.* **2007**, *104*, 20719–20724; f) S. Ihle, O. Onaca, P. Rigler, B. Hauer, F. Rodríguez-Ropero, M. Fioroni, U. Schwaneberg, *Soft Matter* **2011**, *7*, 532–539.

[11] a) M. Sauer, T. Haefele, A. Graff, C. Nardin, W. Meier, *Chem. Commun.* **2001**, 2452–2453; b) P. Baumann, M. Spulber, O. Fischer, A. Car, W. Meier, *Small* **2017**, *13*, 1603943; c) T. Einfalt, R. Goers, I. A. Dinu, A. Najer, M. Spulber, O. Onaca-Fischer, C. G. Palivan, *Nano Lett.* **2015**, *15*, 7596–7603.

[12] a) F. Itel, M. Chami, A. Najer, S. Lörcher, D. Wu, I. A. Dinu, W. Meier, *Macromolecules* **2014**, *47*, 7588–7596; b) F. Itel, A. Najer, C. G. Palivan, W. Meier, *Nano Lett.* **2015**, *15*, 3871–3878.

[13] S. Hernandez-Ainsa, U. F. Keyser, *Nanoscale* **2014**, *6*, 14121–14132.

[14] L. Messager, J. R. Burns, J. Kim, D. Cecchin, J. Hindley, A. L. Pyne, J. Gaitzsch, G. Battaglia, S. Howorka, *Angew. Chem. Int. Ed.* **2016**, *55*, 11106–11109; *Angew. Chem.* **2016**, *128*, 11272–11275.

[15] a) K. Gopfrich, C. Y. Li, M. Ricci, S. P. Bhamidimarri, J. Yoo, B. Gyenes, A. Ohmann, M. Winterhalter, A. Aksimentiev, U. F. Keyser, *ACS Nano* **2016**, *10*, 8207–8214; b) S. Krishnan, D. Ziegler, V. Arnaut, T. G. Martin, K. Kapsner, K. Henneberg, A. R. Bausch, H. Dietz, F. C. Simmel, *Nat. Commun.* **2016**, *7*, 12787; c) R. P. Thomsen, M. G. Malle, A. H. Okholm, S. Krishnan, S. S. Bohr, R. S. Sorensen, O. Ries, S. Vogel, F. C. Simmel, N. S. Hatzakis, J. Kjems, *Nat. Commun.* **2019**, *10*, 5655; d) T. Diederichs, G.

ChemSystemsChem

Research Article
doi.org/10.1002/syst.202200009

**Chemistry
Europe**
European Chemical
Societies Publishing

Pugh, A. Dorey, Y. Xing, J. R. Burns, Q. Hung Nguyen, M. Tornow, R. Tampe, S. Howorka, *Nat. Commun.* **2019**, *10*, 5018.

[16] a) J. R. Burns, A. Seifert, N. Fertig, S. Howorka, *Nat. Nanotechnol.* **2016**, *11*, 152–156; b) P. M. Arnott, S. Howorka, *ACS Nano* **2019**, *13*, 3334–3340; c) C. Lanphere, P. M. Arnott, S. F. Jones, K. Korlova, S. Howorka, *Angew. Chem. Int. Ed.* **2020**; d) C. Lanphere, D. Offenbartl-Stiegert, A. Dorey, G. Pugh, E. Georgiou, Y. Xing, J. R. Burns, S. Howorka, *Nat. Protoc.* **2021**, *16*, 86–130.

[17] J. R. Burns, N. Al-Juffali, S. M. Janes, S. Howorka, *Angew. Chem. Int. Ed.* **2014**, *53*, 12466–12470; *Angew. Chem.* **2014**, *126*, 12674–12678.

[18] a) M. Garni, T. Einfalt, R. Goers, C. G. Palivan, W. Meier, *ACS Synth. Biol.* **2018**, *7*, 2116–2125; b) A. Belluati, S. Thamboo, A. Najer, V. Maffeis, C. von Planta, I. Craciun, C. G. Palivan, W. Meier, *Adv. Funct. Mater.* **2020**, *30*, 2002949.

[19] a) M. Garni, S. Thamboo, C. A. Schoenenberger, C. G. Palivan, *Biochim. Biophys. Acta Biomembr.* **2017**, *1859*, 619–638; b) H. Che, J. C. M. van Hest, *ChemNanoMat* **2019**, *5*, 1092–1109; c) C. Edlinger, T. Einfalt, M. Spulber, A. Car, W. Meier, C. G. Palivan, *Nano Lett.* **2017**, *17*, 5790–5798.

[20] M. Langecker, V. Arnaut, T. G. Martin, J. List, S. Renner, M. Mayer, H. Dietz, F. C. Simmel, *Science* **2012**, *338*, 932–936.

[21] J. Prinos, C. Panayiotou, *Polymer* **1995**, *36*, 1223–1227.

[22] P. Walde, K. Cosentino, H. Engel, P. Stano, *ChemBioChem* **2010**, *11*, 848–865.